Multi-delay photonic correlator for wideband RF signal processing

Guillaume Bourdarot, Jean-Philippe Berger, Hugues Guillet de Chatellus

Research Article Vol. 9, No. 4 / April 2022 / Optica 325

Multi-delay photonic correlator for wideband RF signal processing

Guillaume Bourdarot,[1,2] Jean-Philippe Berger,[2] and Hugues Guillet de Chatellus[1,*]

[1]Laboratoire Interdisciplinaire de Physique, UGA/CNRS, 38000 Grenoble, France
[2]Institut de Planétologie et d'Astrophysique de Grenoble, UGA/CNRS, 38000 Grenoble, France
*Corresponding author: hugues.guilletdechatellus@univ-grenoble-alpes.fr

Received 13 September 2021; revised 14 January 2022; accepted 28 January 2022; published 24 March 2022

Correlation of radio-frequency (RF) signals is a fundamental operation in many fields such as information processing, detection, and imaging techniques at large. Because of the intrinsic limitations of electronic techniques, standard digital correlators, which rely on the acquisition of signals and their processing, become very complex to implement for the real-time analysis of signals whose bandwidth exceeds a few hundred MHz. On the other hand, analog correlators are limited by the performances of RF components. In this paper, we report the proof-of-concept of a correlator architecture based on a simple photonic platform, suitable for analog wideband RF signal processing. The concept, based on multi-heterodyne interferometry, gives access in real time to the entire correlation function of two signals by computing the cross correlation coefficients for 200 values of their relative delay simultaneously. The time-delay step can be adjusted from a few ns down to a few ps, enabling us to process signals with MHz to multi-GHz bandwidth. We have applied this architecture to the localization of RF transmitters by time difference of arrival (TDoA) and obtained a precision close to 10 ps for a 100 ms integration time. This concept is expected to find practical applications in various domains, from radar and electronic warfare to telecommunications, imaging, and radio-astronomy.

https://doi.org/10.1364/OPTICA.442906

1. INTRODUCTION

Correlation is a general concept that characterizes the degree of similarity between data sets. It finds many practical applications in information processing, for statistical analysis, pattern recognition, classification, and data extraction tasks [1]. Correlation is also particularly useful for processing time-dependent signals. If one considers two real signals $s_1(t)$ and $s_2(t)$, the cross correlation (CC) function defined as $C_{1,2}(\tau) = \langle s_1(t)s_2(t+\tau)\rangle$ (where $\langle\rangle$ stands for an average over a given time-window) quantifies the mutual degree of correlation of the two signals as a function of their relative time delay τ. Determining the value of τ that maximizes the degree of correlation is at the basis of time-delay analysis employed in numerous detection and imaging techniques [2]. In active techniques such as radar, lidar, or sonar, the distance to the target is deduced from the measurement of the time of flight (ToF) from the transmitter to the target [3]. In passive systems such as global positioning systems and radio-location systems at large, the position of the receiver can be inferred from time difference of arrival (TDoA) analysis of signals emitted by several transmitters, whose positions are known [45]. Conversely, TDoA makes it possible to locate transmitters by comparing the signals received at different locations, a concept employed in various applications, e.g., for locating natural disaster victims, hunting down interference in mobile communication networks, tracking radio-frequency (RF) jammers, or identifying threats in a war zone [5,6]. In both ToF and TDoA, when short pulsed signals are transmitted, location information is generally obtained from direct measurement of the signal times of arrival. On the contrary, in the case of long or continuous transmitted waveforms, correlation is employed, since it makes it possible to retrieve a temporal resolution limited by the bandwidth of the transmitted waveform, rather than by its duration [2]. In addition, the process of correlation is closely related to convolution and to matched filtering, a feature that guarantees the optimization of the SNR in the case of additive stochastic noise [7]. Finally, beside simple time-delay analysis, a deeper analysis of the correlation function can be useful for advanced high-resolution imaging techniques, such as aperture synthesis in radio-astronomy [8].

For all these reasons, the development of correlators for RF signals is a major challenge. Beyond simplicity and low size, weight, power, and cost, a significant requirement of correlators is their capability to process broadband signals in real time. Indeed, depending of the targeted application, broadband signals are intrinsically related to a high density of information and to a high temporal resolution. Additionally, real-time capability is an important feature of correlation, in order to avoid blind times and to offer a 100% probability of interception. This capability is particularly important for defense applications, or for the observation of low intensity sources in radio-astronomy, among others.

In practice, many correlation techniques have been used so far, both in the frequency and in the time domain. Nowadays,

most of correlation techniques are digital, where the signals are quantized and digitized in discrete data series [9]. Frequency domain approaches are based on the Wiener–Khinchin theorem, which states that the CC function can be retrieved from the inverse Fourier transform (FT) of the product $\tilde{s}_1(f)\tilde{s}_2^*(f)$, where $\tilde{s}_1(f)$ and $\tilde{s}_2(f)$ are the respective FTs of $s_1(t)$ and $s_2(t)$. In time domain approaches, the CC function is calculated by term-by-term products and successive relative shifts of the two series. However, in practice, digital CC in real time is constrained by two limitations. First, according to the sampling theorem, digital processing of wideband signals requires a sampling rate higher than twice the signal bandwidth. Digitizers with sampling rates exceeding a few tens of GS/s are commercially available, but their effective number of bits is severely constrained by the jitter of the clock signal [10]. Second, such data rates are still way beyond the limits of conventional real-time processing techniques. Indeed, the bandwidth of commercial real-time analyzers does not exceed a few hundreds of MHz [11]. These two constraints set a compromise between the signal bandwidth and the probability of interception. In practice, cutting edge applications can overcome these limitations, but at the price of a high degree of complexity: to give an example, the state-of-art Atacama Large Millimeter/Submillimiter Array (ALMA) correlator uses more than 100 millions of processors to process in real time all 8 GHz bandwidth signals coming from 66 antennas [12].

On the contrary, analog approaches are *a priori* very attractive because they do not require acquisition of the signals, nor digital processing. Analog correlation of RF signals can be performed in the frequency domain, a feature widely employed in radar and sonar, where the received signal passes through the matched filter, achieving pulse compression [3] [Fig. 1(a)]. However, in practice, the technique is restricted to the cases where the signal to be detected (i.e., the matched filter) is known. Moreover, this technique is not easily reconfigurable. In turn, time domain analog correlators have been used in the early days of radio interferometry [8], as well as in heterodyne optical interferometry [13]. The product of the signals is calculated by a square-law detector, and the duration of the time-average window is set by the detector response time and by additional low-pass (LP) filters. Time domain approaches are intrinsically sequential: the measurement of the CC function is done point by point by varying the relative time delay between the signals [Fig. 1(b)]. In addition to the technical challenge related to the control of the relative time delay by moving parts, this mode of operation renders the technique intrinsically slow and unsuitable for non-stationary signals. To lift this limitation, parallelized correlation schemes, or lag correlators, have been reported: they enable us to calculate the correlation function for several values of the delay (or lags) simultaneously [Fig. 1(c)] [14,15]. However, this architecture requires as many detectors as lags, which limits in practice the number of lags to a few tens. Generally speaking, despite their potential advantages, analog CC techniques remain less developed than digital ones, mostly because of the poor bandwidth acceptance of analog RF components and because of the limited scalability of RF analog circuits.

Recently, the field of photonics has proven to offer efficient solutions for analog processing of wideband RF signals by taking advantage of the huge bandwidth of the optical spectrum and of the availability of cheap and high-performance components at the telecom wavelength [16,17]. Moreover, photonic architectures are immune to electromagnetic interference. Microwave photonics

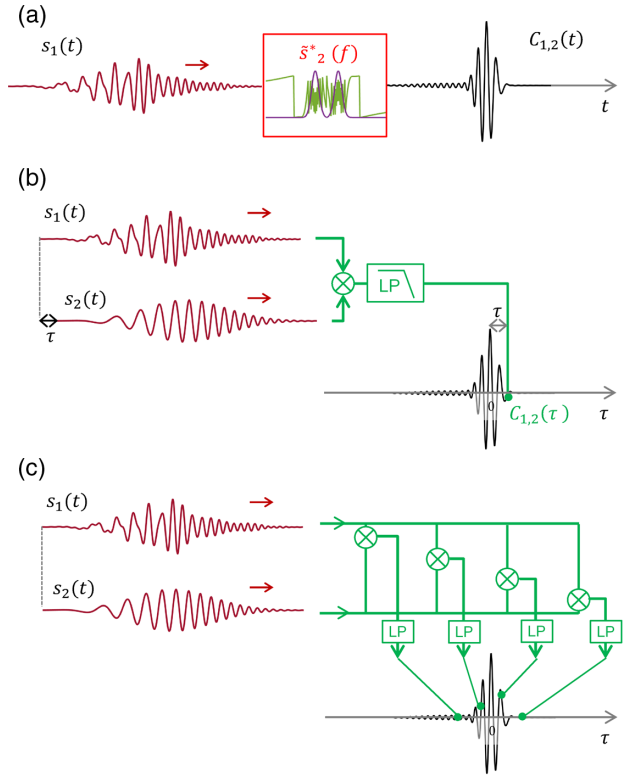

Fig. 1. (a) Analog cross correlation (CC) of two signals $s_1(t)$ and $s_2(t)$ in the frequency domain. $s_1(t)$ passes through a filter, whose transfer function is the complex conjugate of $\tilde{s}_2(f)$ (magenta, amplitude; green, phase). The output signal is $C_{1,2}(t)$. When $s_1 = s_2$, the process corresponds to auto-correlation (AC), or matched filtering. (b) Analog CC in the time domain. Analog multiplication of the signals time-shifted by τ is followed by low-pass filtering (LP) to calculate the CC coefficient $C_{1,2}(\tau)$. The measurement is repeated while varying the delay, to reconstruct the whole CC function $C_{1,2}(\tau)$. (c) Analog lag correlator. The measurement of the CC coefficients is performed for several (here, four) values of the relative delay of the input signals simultaneously (see text).

has, thus, emerged and greatly developed in the past decades [18]. Besides, correlation is a common process in optics: it is at the heart of FT spectroscopy [19] and aperture synthesis in optical stellar interferometry [20], while non-linear auto-correlation (AC) techniques are widely used to characterize ultra-short optical pulses [21]. Therefore, several photonic-aided approaches have been proposed for RF signal correlation so far, and they have demonstrated the capability of processing multi-GHz-wide signals. Implementation in the spectral domain rely generally on the use of tailored linear filters [22–24], while temporal approaches make use of non-linear techniques [25–28], or of direct up-conversion of the RF signal to the optical domain followed by photodetection [29]. Other architectures of correlators based on free-space optics have been demonstrated in the frame of optical computing [30,31], and adapted to the correlation of millimeter-waves by frequency up-conversion [32–34]. Finally, wideband correlators based on diffraction in cryogenically cooled crystals doped with rare-earth ions have been developed and commercialized [35,36]. However, generally speaking, photonic solutions turn to have the same limitations as analog electronic ones: a high degree of complexity, a lack of reconfigurability in spectral approaches, and the need for point-by-point measurements in temporal ones.

In this paper, we propose a novel analog correlation technique of RF signals based on a simple photonic architecture, which surpasses the capabilities of analog and digital conventional techniques. The proposed system interprets as a lag correlator based on photonics: it relies on the multiplexing of the relative delay between the input signals τ, which avoids the need for point-by-point measurements of the CC function (no moving part), and makes it possible to calculate the entire correlation function in parallel (i.e. for about 200 values of the delay τ simultaneously). Like in lag correlators, the correlation is computed on the fly (i.e. in real time), without any truncation of the input signal. But contrary to conventional lag correlators, the architecture requires a single detector, and it is easily reconfigurable: the time-delay step can be controlled over orders of magnitude down to the ps scale, enabling the processing of multi-GHz wideband signals [37].

The paper is structured as follows. First, we provide a concise description of the photonic correlator. Then, we report both AC and CC of arbitrary RF signals. In particular, we demonstrate the reconfigurability of the architecture by performing CC with three different values of the time-delay step (125 ps, 4 ns, and 23 ps). Next, we characterize the performance of the architecture for time-delay analysis of RF signals and report a precision approaching 10 ps for a 100 ms integration time. Then, we provide a practical demonstration of transmitter localization by TDoA. In the conclusion, we discuss the perspectives and the limitations of the technique for practical applications. Supplement 1 regroups complementary theoretical and experimental details on the operation of the correlator, as well as additional examples of correlation measurements.

2. ARCHITECTURE OF THE PHOTONIC CORRELATOR

In this part, we provide a brief description of the correlator (Fig. 2). Its principle is the following. We consider two input RF signals, $s_1(t)$ and $s_2(t)$, feeding continuously the system. Both of them are transferred into the optical domain, where they are duplicated to produce a large number ($N > 200$) of periodically time-shifted replicas. The values of the time shifts for the two signals are different and are written τ_1 and τ_2 for $s_1(t)$ and $s_2(t)$, respectively. Moreover, the time-delayed replicas of the signals are simultaneously shifted in frequency so that the replica that has been delayed n times has also experienced n frequency shifts: in other words, the time delays of the signal replicas are mapped in the frequency domain. Similarly, the frequency shifts are slightly different and are, respectively, noted f_1 and f_2. The replicas of the two signals are combined on a photodiode (which plays the role of the square-law detector) followed by a LP filter. Fourier processing of the photocurrent gives access to the CC coefficients of the two signals.

The practical implementation of this concept utilizes a pair of frequency shifting loops, or FSLs [38]. A (single) FSL consists of a fiber loop containing a frequency shifter (usually, an acousto-optic frequency shifter, or AOFS), an amplifier to compensate for the losses of the system (here, an erbium-doped fiber amplifier, EDFA), and a tunable bandpass filter (TBPF). The role of the filter is to limit the amplified spontaneous emission (ASE) of the amplifier and to control the spectral bandwidth, i.e., N the number of round trips of the light in the loop. The FSL can be seeded by a CW laser (frequency, f_0), modulated in amplitude by the RF signal under test, owing to a single-ended Mach–Zehnder modulator, or amplitude modulator (AM) biased at the null point. In this case, the FSL generates replicas of the RF input signal (transferred in the optical domain). The time shift of the replicas is simply equal to the travel time in the loop, while their separation in frequency is equal to the frequency shift per turn in the loop. Recall that, as such, FSLs have proven many applications in the field of microwave photonics for the processing and the generation of RF signals [39–43], as well as in spectroscopy and ranging [44,45].

Here, the correlator architecture involves a pair of FSLs, whose travel times are τ_1 and τ_2. We define $\Delta\tau = \tau_2 - \tau_1$. The frequency shifts per turn are equal, respectively, to f_1 and f_2 (both close to 80 MHz), and we define similarly $\Delta f = f_1 - f_2$. The values of the frequency shifts are sufficiently close, to match the condition $N\Delta f < f_2/2,\ f_1/2$. The two FSLs are seeded by the same CW laser (1550 nm), modulated by $s_1(t)$ and $s_2(t)$, respectively. In order to preserve the optical coherence between the signals and to limit the effects of mechanical or thermal drifts on the fiber lengths, the FSLs are implemented in a bidirectional configuration [46,47]. The two signals travel in opposite directions in the same fiber loop, except a short non-reciprocal section where they experience different time delays and frequency shifts (inset of Fig. 2). Output couplers enable to extract a fraction of the counterpropagating signals.

It can be shown that, after the output couplers, the electric fields $E_1(t)$ and $E_2(t)$ write

$$E_{1,2}(t) = E_0 e^{i2\pi f_0 t} \sum_{n=0}^{N} s_{1,2}(t - n\tau_{1,2}) e^{i2\pi n f_{1,2} t} e^{-i\pi f_{1,2}\tau_{1,2} n^2}. \tag{1}$$

Both fields are recombined on a balanced photodetector. The photocurrent passes trough a LPfilter (cutoff frequency, $N\Delta f$). Calculations derived in Supplement 1 show that, for most signals, the photocurrent, defined in complex formalism, by $I(t) \propto E_1(t) E_2^*(t)$ writes, after LP filtering, the following:

$$I(t) \propto \sum_n \langle s_1(t) s_2(t - n\Delta\tau)\rangle e^{i2\pi n\Delta f t} e^{-i\pi(f_1\tau_1 - f_2\tau_2)n^2}. \tag{2}$$

This expression shows that the CC function sampled at multiples of $\Delta\tau$ can be retrieved by computing the FT of $I(t)$,

$$\tilde{I}(n\Delta f) \propto \langle s_1(t) s_2(t - n\Delta\tau)\rangle e^{-i\pi(f_1\tau_1 - f_2\tau_2)n^2}. \tag{3}$$

In other words, the CC function is mapped in the RF spectrum (i.e., the FT of the photocurrent): the amplitude of the heterodyne beatnote at frequency $n\Delta f$ is proportional to the value of the CC function at a relative delay $n\Delta\tau$.

Advantageously, the system parameters can be adjusted so that $f_1\tau_1 - f_2\tau_2$ is an even integer. In this case, the FT of the photocurrent after filtering provides directly the CC function of the input signals. When this condition is not met, the square modulus of the FT of the photocurrent provides only the square of the CC function. Interestingly, the operation mode of the correlator is closely related to multi-heterodyne interferometry as implemented in dual-comb techniques [48,49]: the information sought (here, the CC coefficients; in dual-comb techniques, the amplitude and phase of the comb lines) is contained in the low frequency beatnotes in the RF spectrum produced by the interference of the teeth of the first comb, with their closest neighbor (in terms of frequency) in the second one.

As said, the sampling time-delay step of the CC function $\Delta\tau$ is directly set by the path difference of the bidirectional FSL. In

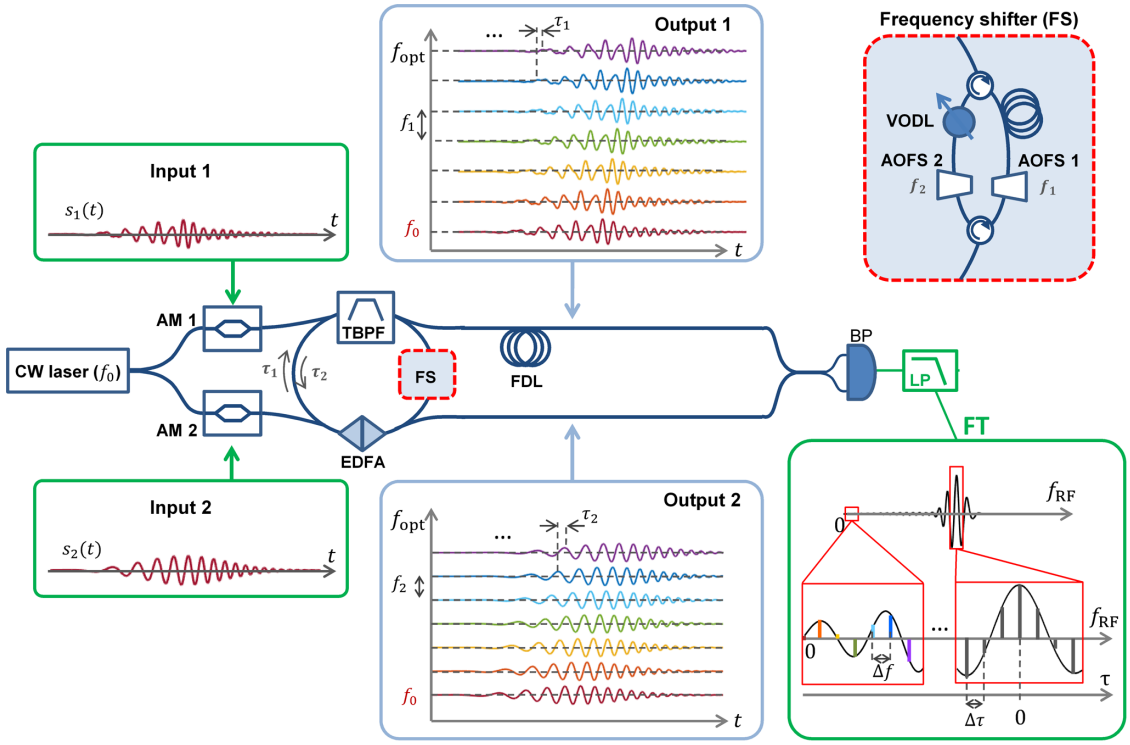

Fig. 2. Sketch of the analog photonic correlator. A bidirectional fiber frequency shifting loop (FSL) is seeded in both ways by a CW laser at 1550 nm, modulated in amplitude (AM) by two RF signals $s_1(t)$ and $s_2(t)$. Two variable optical attenuators (not shown) enable us to control the light power injected in the loop. The non-reciprocal frequency shifter (FS) is sketched in the inset (top right). A variable optical delay line (VODL) enables to control the time delay between both ways $\Delta\tau = \tau_2 - \tau_1$. The loop contains an amplifier (EDFA) and a tunable bandpass filter (TBPF), both bidirectional. The loop produces replicas of the input signals transferred in the optical domain, shifted both in time and in frequency. Photodetection by the balanced detector (BP) produces multi-heterodyne beatings. After low-pass filtering (LP), the Fourier transform (FT) of the photocurrent (i.e., the RF spectrum) sampled at multiples of $\Delta f = f_1 - f_2$ provides the CC coefficients for values of the relative delay multiples of $\Delta\tau$ (see text). A fiber delay line (noted FDL) is inserted in path #1 at the FSL output, in order to bring the position of the null delay (i.e., $\tau = 0$) to the center of the RF spectrum.

practice, this value can be precisely tuned by means of a variable optical delay line (VODL). It can be set arbitrarily small, leading to the possibility of processing signals with tens of GHz bandwidth. Ultimately, the processing bandwidth is limited by the bandwidth of the TBPF inserted in the loop, i.e., Nf_1 ($\simeq Nf_2$). Typically, this value approaches 20 GHz (assuming $N = 250$ and $f_1 \simeq 80$ MHz). The advantage of the system is the capability to compute, simultaneously and in real time, the CC coefficients for more than 200 values of the delay simultaneously, with no moving part, and with a single detector. Therefore, the technique is not restricted to stationary signals but can also be applied to the processing of time-dependent signals, provided that their change rate is smaller than the processing time of the system. The latter is about $N\tau_1$ ($\simeq N\tau_2$), typically close to 20 μs ($N = 200$ and $\tau_1 \simeq 100$ ns).

3. EXPERIMENTAL RESULTS

In a first set of experiments, we demonstrate the capability of the setup to measure the entire AC and CC functions of different input RF signals.

A. Examples of Cross- and Auto-Correlation of RF Signals

We have implemented the photonic correlator with three different values of the time-delay step $\Delta\tau$. In the first case, $\Delta\tau$ is set to 115 ps. This configuration is suitable for signal correlation, the bandwidth of which can be up to 4 GHz. Considering $N = 200$, the total delay range between the two input signals reaches $N\Delta\tau = 23$ ns. In order to measure a CC function whose zero delay corresponds to the center of the RF spectrum of the photocurrent, we compensate the paths mismatch by inserting about 3 m of fiber on the path of the output #1 (FDL in Fig. 2). To satisfy the condition $f_1\tau_1 = f_2\tau_2$, f_1 and f_2 are, respectively, equal to 80.0657 and 80.0000 MHz ($\Delta f = 65.7$ kHz). The cutoff frequency of the LP filter is set to 15 MHz. The filtered photocurrent is digitized by means of a oscilloscope at 50 MSa/s. The FT is computed numerically, using a Blackman–Harris window.

First, we measure the AC functions of simple waveforms (white noise and sine waves). The amplitude of the applied voltage is chosen smaller than the V_π on the AMs (5 V), to avoid non-linearities and distortion of the correlation function. In practice, the peak-to-peak voltage of the input signal is lower than 1 V. In Fig. 3(a), we show the RF power spectra obtained by seeding the system with white noise of variable bandwidth (from 120 MHz down to 40 MHz). The traces consist of well-defined beatnotes (more than 200), whose power is proportional to the square of the AC coefficient. The beatnotes dominate a noise background that mostly comes from the ASE circulating in the FSL. Since the frequency of the beatnotes is precisely known (their frequency is an integer multiple of Δf), the noise background can readily be filtered out numerically. In most of the data shown in the following of the paper, this filtering has been implemented. As said, the relationship

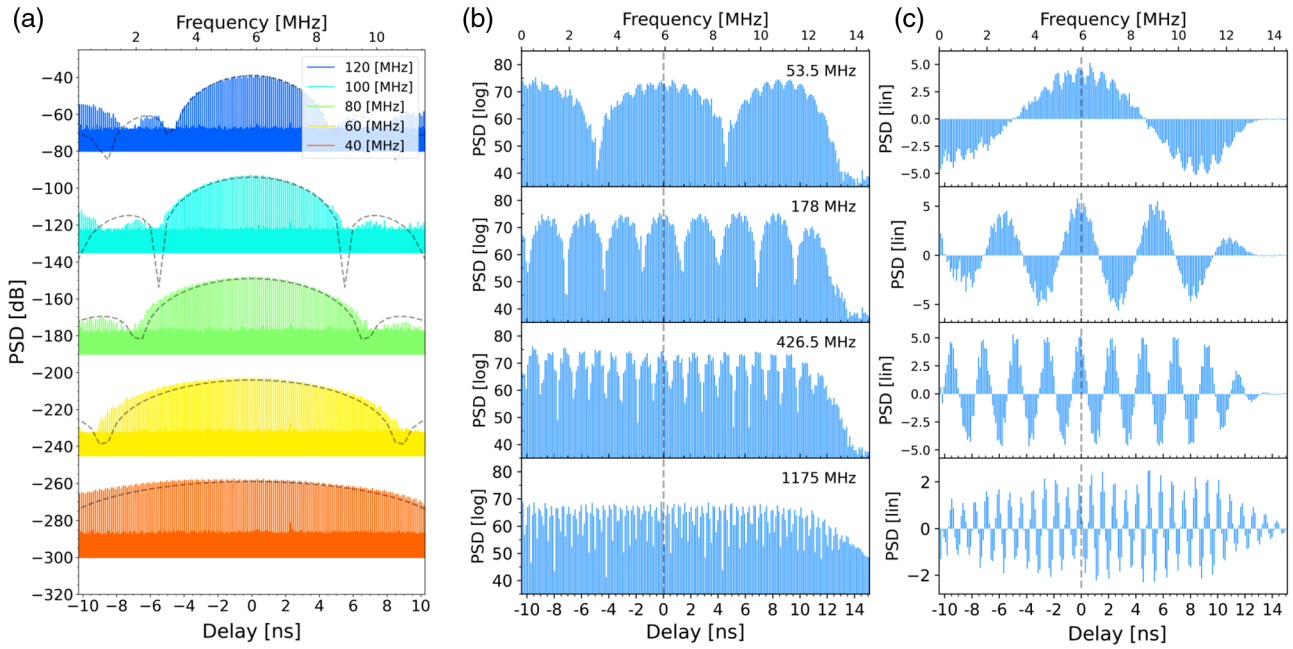

Fig. 3. (a) Square modulus of the AC of a white noise with different bandwidths (120 MHz to 40 MHz) (acq. time, 200 ms, log. scale). The dashed line is the expected (numerical) AC trace. (b) Square modulus of the AC of sine waves with different frequencies (log. scale, acq. time: 100 ms). The noise background in the AC traces has been numerically filtered out (see text). The residual modulations in the traces are due to sampling effects in the RF spectrum. (c) Real part of the AC (linear scale) of the previous sine waves. The vignetting in the real part traces comes from a small residual quadratic phase in the RF spectrum.

between the frequency axis of the RF spectrum and the time delay is linear, with a proportionality coefficient equal to $\Delta f/\Delta\tau$. As expected, the width of the AC function (i.e., the coherence time of the applied signal) decreases with the spectral bandwidth of the signal. We also compare the AC traces obtained by the photonic correlator, with the expected ones. The latter are calculated by recording the RF signal with a fast digital oscilloscope and computing the AC function. A good agreement is found between the experimental and the expected traces. In Fig. 3(b), we plot the AC functions of sine waves with different frequencies. Interestingly, since $\tilde{I}(f)$ maps the real part of the AC function, it is possible to retrieve the sign of the AC function. Examples of real values of the AC function are plotted in Fig. 3(c).

In Fig. 4, we demonstrate the capability of the setup for CC. Two different RF signals are used: the first one is a 120 MHz bandwidth digitally synthesized white noise, the second one is the same signal after notch filtering (stopband, 65–85 MHz). The spectra of the input RF signals are displayed in Fig. 4(a). In Fig. 4(b), we recall the AC traces obtained separately with each of these signals. Then, both signals are sent to the system, and the experimental CC trace is shown in Fig. 4(c). Similarly to the previous case, the expected CC trace is computed numerically and plotted for comparison. Notice that, contrary to the AC traces, CC traces do not necessarily exhibit their maximum at zero delay.

As said, depending on the signal under test, the time-delay step is simply reconfigurable by changing the optical path delay $\tau_2 - \tau_1$. To show the flexibility of the concept, we have increased the value of the time-delay step by inserting 1 m of optical fiber next to AOFS 2. (Simultaneously, to bring the position of the null relative delay at the center of the RF spectrum, we have added a 100 m long fiber delay line on the path of output #1.) In this case, the value of $\Delta\tau$ is about 4 ns, which makes this configuration suitable for

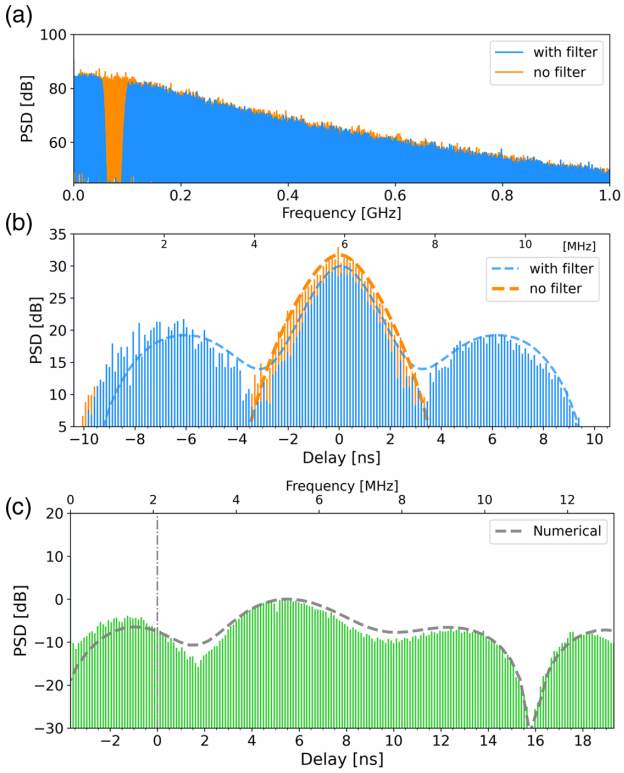

Fig. 4. (a) Spectrum of a 120 MHz bandwidth digitally synthesized noise, in orange, and of the same signal after a bandstop filter (65–85 MHz), in blue. (b) Square modulus of the ACs of both signals (acq. time, 200 ms). (c) CC trace between the unfiltered and the filtered signal (acq. time, 200 ms). In all plots, the experimental AC and CC traces are compared to the expected ones (in dashed line).

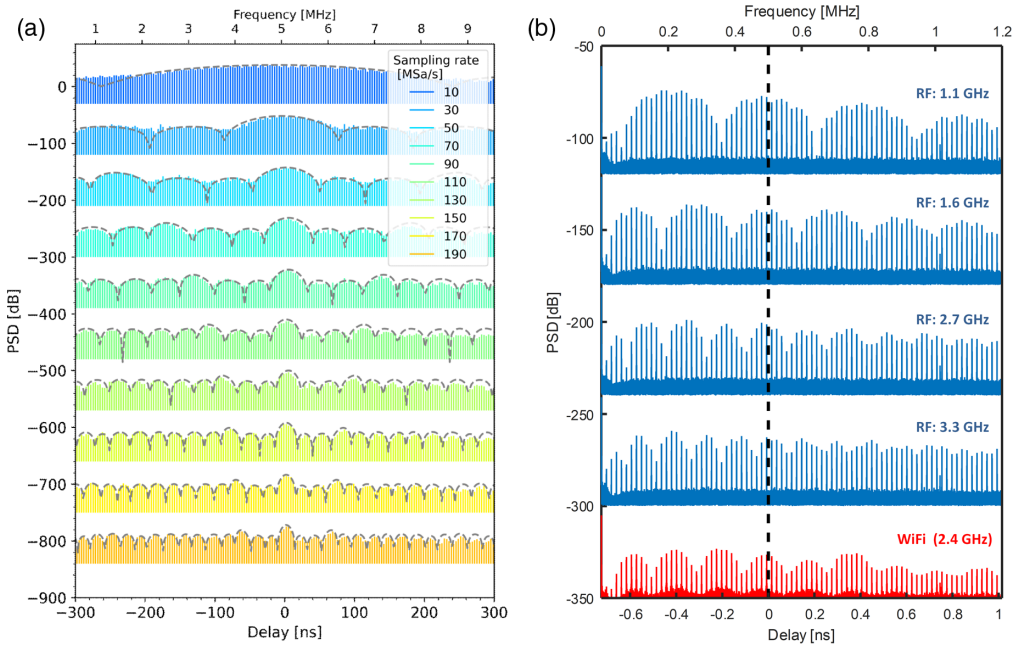

Fig. 5. (a) Solid lines, experimental AC traces of a specifically designed noise-like input signal. The time step of the correlator is set to $\Delta\tau = 4$ ns. The sampling rate of the input signal is increased, from 10 to 190 MSa/s. Dashed lines are the expected AC traces (acq. time, 100 ms). (b) Experimental AC traces of high-frequency signals. The time step of the correlator is set to $\Delta\tau = 23$ ps. The traces in blue correspond to the AC of pure sine waves with frequencies ranging from 1.1 to 3.3 GHz. The red trace is obtained with the signal emitted by a WiFi repeater, captured by a broadband antenna and amplified before being sent into the correlator (acq. time, 100 ms).

signals with a bandwidth up to 125 MHz. The maximum delay range is now close to 0.8 μs. A numerical signal has been specifically designed, so as to exhibit a relatively complex AC function with many sidelobes. This noise-like signal is sent to the system with different sampling rates (from 10 to 190 MSa/s), so as to vary its bandwidth. The results are displayed in Fig. 5(a). In this case too, the experimental traces obtained through the analog photonic correlator show an excellent agreement with the numerical correlation traces. Similarly, we have also configured the system to process signals with multi-GHz bandwidth. For this aim, the delay time step is reduced down to 23 ps by proper adjustment of the VODL. Waveforms with frequencies ranging from 1.1 to 3.3 GHz are sent to the AMs. In these experiments, the value of Δf is set to 15 kHz. The cutoff frequency of the LP filter is 1.9 MHz, and the sampling rate of the oscilloscope is 10 MSa/s. The AC traces are shown in Fig. 5(b) (in blue). Additionally, to prove the capability of the system to correlate high-frequency signals in real time, we connect a broadband antenna and a set of two RF amplifiers (55 dB total gain at 1 GHz) to the AMs. The antenna is directed towards a WiFi repeater. The AC trace, displayed in red [Fig. 5(b)], shows a periodic variation characteristic of the WiFi frequency band at 2.4 GHz.

Finally, we briefly discuss the sensitivity of the correlator. To ensure a good signal-to-noise ratio (SNR, i.e., higher than 30 dB for a 100 ms acquisition time), the power of the RF signal at the modulator input is typically 3 dBm. Since the power at the correlator output scales as the square of the input one (see Supplement 1), the sensitivity (the minimum power of the input signal corresponding to a SNR equal to unity) is −12 dBm for a 100 ms acquisition time).

B. Time-Delay Analysis

A major application of signal correlation is the possibility to measure the time delay T between two mutually delayed replicas of the same signal (written as $s(t)$ and $s(t-T)$). The value of τ that maximizes $\langle s(t)s(t-T+\tau)\rangle$ is simply equal to T, the time delay. As said, the main advantage of time-delay analysis based on correlation is the matched filtering effect: the delay information is contained in a correlation peak, whose duration is set by the spectral bandwidth of the signal [2]. This peak can be very narrow, even in the case of quasi CW signals. As said, this pulse compression effect is particularly useful to enhance the SNR, e.g., in radar techniques based on matched filtering. Here, the system offers the capability to perform such time-delay measurements directly in the time domain. To demonstrate this feature, we apply to the AMs two mutually delayed replicas of the same signal (a numerically synthesized white noise with a 120 MHz bandwidth). The relative time delay between the replicas is controlled digitally. We record the CC traces for different values of the time delay. As expected, the delay measured through the photonic correlator matches closely the digital delay applied to the input signals [Fig. 6(a)]. Then, we characterize the precision of the time-delay measurement offered by the technique. To do so, we acquire a 1-s-long time trace and clip it numerically into sequences of duration equal to a multiple (labeled by q) of 15.2 μs (i.e., $1/\Delta f$). For each value of q, we calculate the position of the AC peak (i.e., the value of the delay) by a numerical fitting procedure, and we determine the deviation of this measurement repeated over the full-length trace. The results are given in Fig. 6(b). As expected, the deviation decreases as the square root of the integration time. Beyond 100 ms integration times, the experimental results tend to deviate from this law, presumably due to the smaller number of statistical samples available. Nevertheless, the precision is close to 10 ps for 100 ms integration

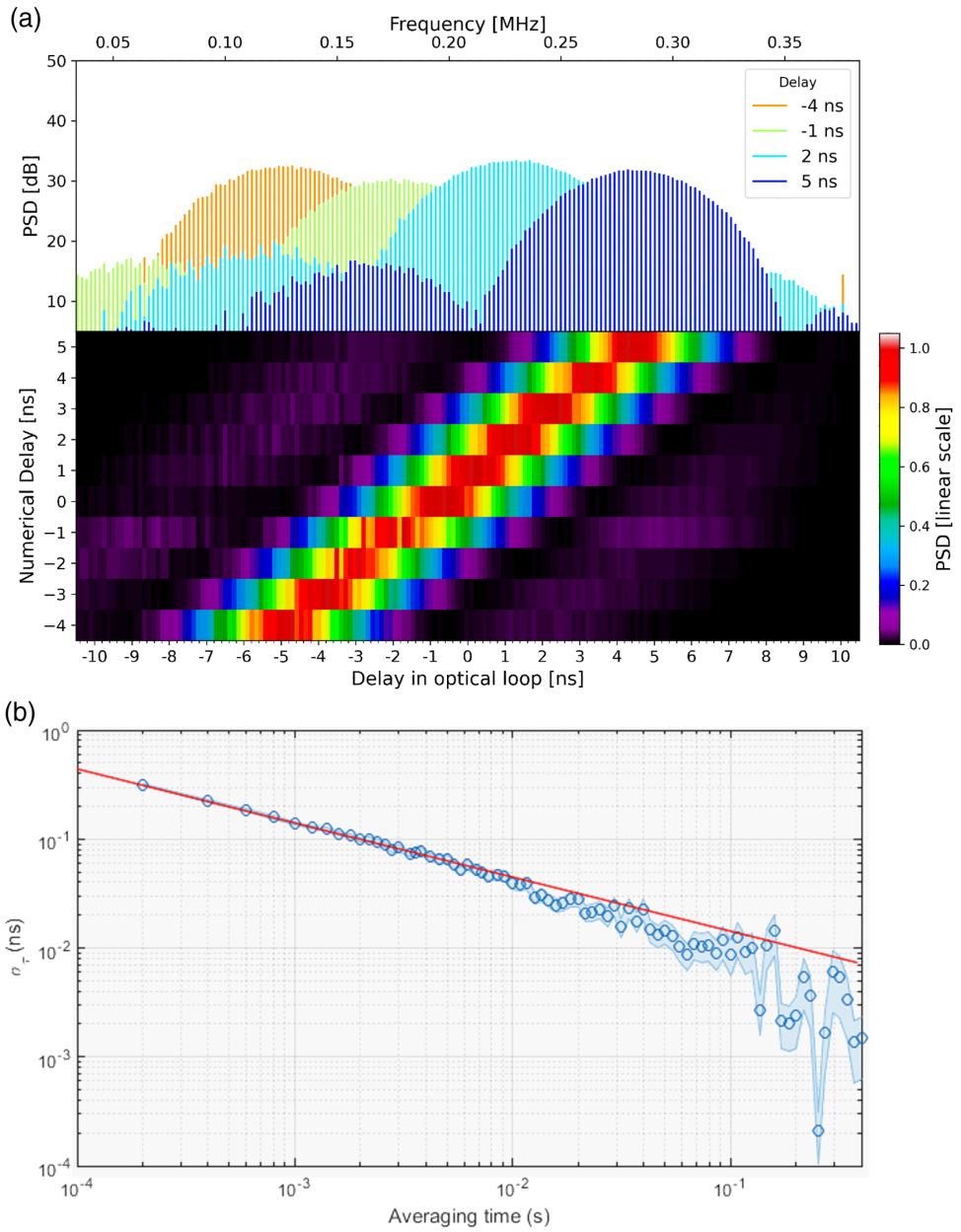

Fig. 6. (a) Top, experimental AC traces measured for time-delayed replicas of a 120 MHz bandwidth white noise. Bottom, 2D plot of the AC traces as a function of the delay. (c) Allan deviation of the time-delay measurement, as a function of the averaging time (see text). The red line is a guide for the eyes (slope, −1/2).

time, a value significantly smaller than the 8.3 ns coherence time of the signal under test (1/120 MHz). It is also much smaller than the mean period of the signal (16.7 ns), which means that the time delay is measured with a precision better than one-thousandth of a wavelength (in 100 ms).

C. Application to Time Difference of Arrival

In a last set of experiments, we demonstrate the capability of the system for the localization of an RF transmitter by TDoA. Here, we provide a 2D proof of concept at the lab scale with a single transmitter and two receivers, but the technique could be generalized to more complex antenna networks, e.g., to implement passive radar by triangulation. A complex broadband noise-like signal is synthesized by combining a white noise generator and frequency multipliers with LP and high-pass filters. The spectrum of the resulting RF signal ranges between 0.4 and 1.2 GHz [Fig. 7(a)]. The RF signal is sent to a whip (monopole) antenna (Tx). Two receiving antennas (Rx1 and Rx2), identical to the transmitter, are placed at a distance of about 1 m from Tx [see Fig. 7(b)]. Rx2 can be moved to change the relative delay between the signals received by the antennas. These two signals are amplified and applied to the AMs at the correlator input. The measured CC functions are displayed in Fig. 7(c). As expected, the CC traces shift with the position of Rx2. In this case also, the delay retrieved from the analog photonic correlation matches precisely the geometrical delay between the antennas, demonstrating the capability of the system for TDoA analysis.

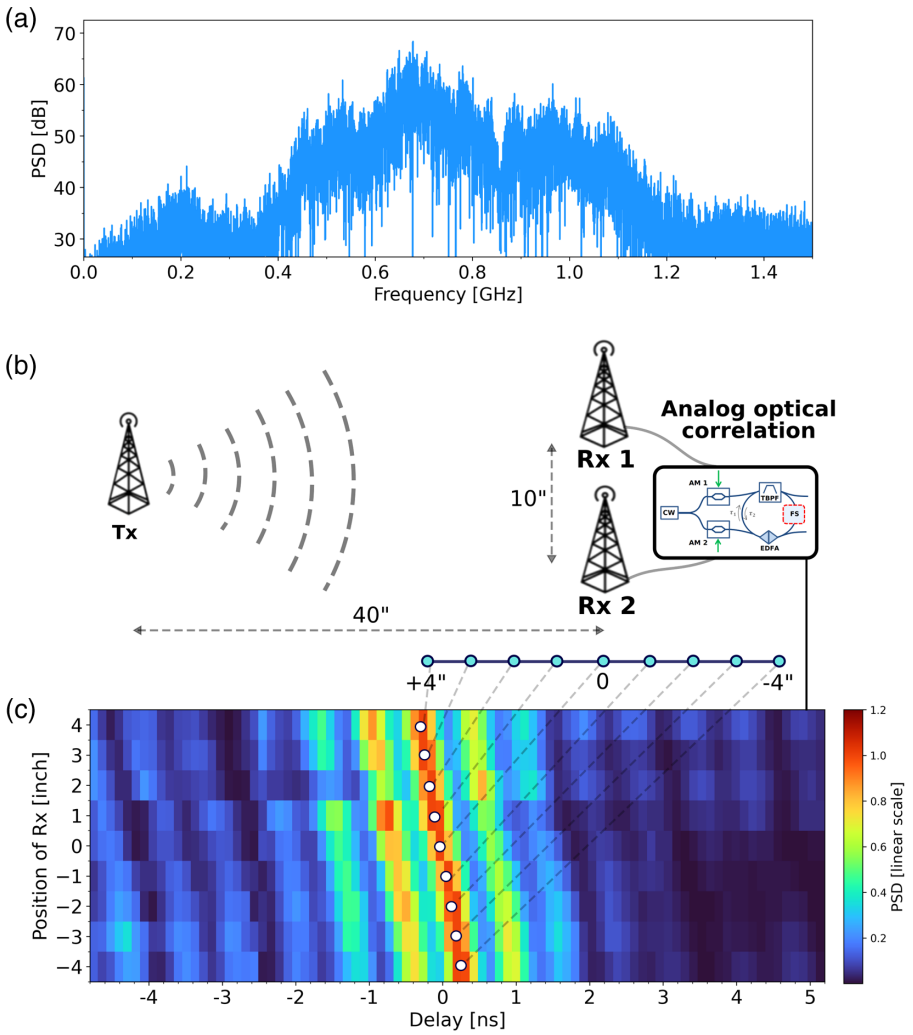

Fig. 7. Proof of concept of TDoA. (a) RF spectrum of the transmitted signal. (b) Sketch of the experimental setup (see text). (c) 2D plot of the CC traces as a function of the positions of Rx2 (100 ms acq. time).

4. CONCLUSION

In this paper, we have reported an analog photonic-based lag correlator that enables us to compute the CC of wideband RF signals for more than 200 values of the delay simultaneously. The architecture is considerably simpler than conventional analog or digital wideband correlators. Here, the optical circuitry is based on off-the-shelf telecom components. No broabdand laser source is needed, but a low linewidth single frequency laser. Contrary to most conventional analog approaches in the time domain that rely on point-by-point measurements of the CC coefficients, our architecture contains no moving part and computes, with a single detector, the CC function as a whole through 200 simultaneous values of the relative delay, enabling real-time signal processing. On a dynamic point of view, the typical computation time of the CC function is about 20 μs, a value significantly lower than any other point-by-point CC technique. This value is also the time response of the correlator. Additionally, the architecture requires a relatively slow detection electronics (lower than 50 MHz bandwidth and 50 MSa/s acquisition rate), orders of magnitude smaller than the frequency of the input RF signals. Finally, recall that no truncation is applied to the input signal, which means that our architecture performs correlation with a 100% probability of interception.

The spectral bandwidth of the signals to be processed is an important parameter of the system. As said, in our architecture it is set by two factors. The first one is the time-delay step. In the reported experiments, it could reach 23 ps, but this value could be arbitrarily smaller. The second limiting factor is the optical spectral bandwidth set by the TBPF (i.e., $Nf_1 \simeq Nf_2$). One could imagine increasing the spectral bandwidth of the filter, which would simultaneously result in an increase of the number N of round trips and of the signal bandwidth supported by the system. However, the saturation of the gain of the amplifier would lead to a decrease of the power as the signal circulates in the loop [50]. The use of frequency shifters with a larger nominal frequency shift (e.g., electro-optic single-sideband frequency shifters) could enable us to increase the filter's spectral bandwidth while keeping the number of round trips constant, avoiding the problem of saturation. This solution could be attractive, but presumably at the cost of increased ASE [50]. In addition to the capability of processing signals with multi-GHz bandwidth, our architecture shows another advantage. In digital techniques, the data collected at each antenna must be accurately time-stamped to accurate clock signals. This requires us to have an absolute time reference shared between all antennas and the correlator. In our architecture, a phase stabilization of the optical link between the antennas and the correlator is sufficient and can

be achieved with standard fiber stabilization techniques. This leads to the possibility of performing signal correlation over very long baselines, a feature that could find promising applications in sub-millimetric interferometry. Additionally, this architecture could also open perspectives in optical interferometry. Infrared heterodyne interferometry, which replaces the correlation of the optical signals received by the telescopes, by the correlation of RF signals obtained by mixing the optical signals with a local oscillator on a photodetector, could benefit from the proposed correlation technique [13,29]. Beside synthetic aperture imaging in astronomy, other applications based on time-delay analysis are conceivable, including passive radar and localization of transmitters/receivers. For most of these applications, the extension of the correlator to more than two signals would represent a significant advantage, e.g., to achieve long baseline interferometry with a large array of antennas or to enable transmitter's localization by triangulation. The extension of the architecture proposed here to more than two signals is underway. In the long term, perspective of integration of this architecture is foreseeable. All components used in the dual FSL, including the frequency shifter, can be integrated [51]. The combination of all components on a single chip could be accessible, presumably via hybrid integration techniques, and could open many possibilities of applications of the architecture.

Funding. Institut national des sciences de l'Univers (ASHRA, CSAA); Université Grenoble Alpes (Ecole Doctorale de Physique, IDEX-IRS 2020).

Acknowledgment. We acknowledge support from Université Grenoble Alpes, from the Ecole Doctorale de Physique de Grenoble, and from the INSU-CNRS (ASHRA and CSAA) for their financial support. We also acknowledge Vicente Duran for his work at the early stages of the system's implementation.

Disclosures. The authors declare no conflicts of interest.

Data availability. Data underlying the results presented in this paper may be obtained from the authors upon request.

Supplemental document. See Supplement 1 for supporting content.

REFERENCES

1. R. S. Witte and J. S. Witte, *Statistics*, 11th ed. (Wiley, 2017).
2. J. Y. Stein, *Digital Signal Processing: A Computer Science Perspective* (Wiley, 2000), Chap. 9.
3. N. Levanon and E. Mozeson, *Radar Signals* (Wiley, 2004).
4. H. D. Griffiths and C. J. Baker, *An Introduction to Passive Radar* (Artech House, 2017).
5. A.-M. Roxin, J. Gaber, M. Wack, and A. N. S. Moh, "Survey of wireless geolocation techniques," *IEEE Globecom Workshops*, Washington, D.C., USA, 2007.
6. H. Liu, H. Darabi, P. Banerjee, and J. Liu, "Survey of wireless indoor positioning techniques and systems," IEEE Trans. Syst. Man Cybern. C **37**, 1067–1080 (2007).
7. R. E. Ziemer and W. H. Tranter, *Principles of Communications* (Wiley, 1988).
8. A. R. Thompson, J. M. Moran, and G. W. Swenson, Jr., *Interferometry and Synthesis in Radio Astronomy*, 3rd ed. (Springer, 2017).
9. S. N. Kuo, B. H. Lee, and W. Tian, *Real-Time Digital Signal Processing: Fundamentals, Implementations and Applications*, 3rd ed. (Wiley, 2013).
10. B. Murmann, "The race for the extra decibel: a brief review of current ADC performance trajectories," IEEE Solid-State Circuits Mag. **7**(3), 58–66 (2015).
11. "Fondamentals of real-time spectrum analysis," Tektronix, 2015, https://download.tek.com/document/37W_17249_5_HR_Letter.pdf.
12. R. P. Escoffier, G. Comoretto, J. C. Webber, A. Baudry, C. M. Broadwell, J. H. Greenberg, R. R. Treacy, P. Cais, B. Quertier, P. Camino, A. Bos, and A. W. Gunst, "The ALMA correlator," Astron. Astrophys. **462**, 801–810 (2006).
13. D. D. S. Hale, M. Bester, W. C. Danchi, W. Fitelson, S. Hoss, E. A. Lipman, J. D. Monnier, P. G. Tuthill, and C. H. Townes, "The Berkeley infrared spatial interferometer: a heterodyne stellar interferometer for the mid-infrared," Astrophys. J. **537**, 998–1012 (2000).
14. C.-T. Li, D. Y. Kubo, W. Wilson, *et al.*, "AMiBA wideband analog correlator," Astrophys. J. **716**, 746–757 (2010).
15. C. M. Holler, M. E. Jones, A. C. Taylor, A. I. Harris, and S. A. Maas, "A 2–20-GHz analog lag correlator for radio interferometry," IEEE Trans. Instrum. Meas. **61**, 2253–2261 (2012).
16. R. A. Minasian, "Photonic signal processing of microwave signals," IEEE Trans. Microwave Theory Tech. **54**, 832–846 (2006).
17. H. Caulfield and S. Dolev, "Why future supercomputing requires optics," Nat. Photonics **4**, 261–263 (2010).
18. D. Marpaung, J. Yao, and J. Capmany, "Integrated microwave photonics," Nat. Photonics **13**, 80–90 (2019).
19. S. P. Davis, M. C. Abrams, and J. W. Brault, *Fourier Transform Spectrometry* (Academic, 2001).
20. J. D. Monnier, "Optical interferometry in astronomy," Rep. Prog. Phys. **66**, 789–857 (2003).
21. C. Monat, C. Grillet, M. Collins, A. Clark, J. Schroeder, C. Xiong, J. Li, L. O'Faolain, T. F. Krauss, B. J. Eggleton, and D. J. Moss, "Integrated optical auto-correlator based on third-harmonic generation in a silicon photonic crystal waveguide," Nat. Commun. **5**, 3246 (2014).
22. M. S. Rasras, I. Kang, M. Dinu, J. Jaques, N. Dutta, A. Piccirilli, M. A. Cappuzzo, E. Y. Chen, L. T. Gomez, A. Wong-Foy, S. Cabot, G. S. Johnson, L. Buhl, and S. S. Patel, "A programmable 8-bit optical correlator filter for optical bit pattern recognition," IEEE Photon. Technol. Lett. **20**, 694–696 (2008).
23. Y. Dai and J. Yao, "Microwave correlator based on a nonuniformly spaced photonic microwave delay-line filter," IEEE Photon. Technol. Lett. **21**, 969–971 (2009).
24. J. Yao, "Photonics to the rescue: a fresh look at microwave photonic filters," IEEE Microw. Mag. **16**(8), 46–60 (2015).
25. R. Kibria, L. A. Bui, and M. W. Austin, "Nonlinear mixing based photonic correlator," in *IEEE International Topical Meeting on Microwave Photonics* (2012), pp. 30–33.
26. M. Ziyadi, M. R. Chitgarha, S. Khaleghi, A. Mohajerin-Ariaei, A. Almaiman, J. Touch, M. Tur, C. Langrock, M. M. Fejer, and A. E. Willner, "Tunable optical correlator using an optical frequency comb and a nonlinear multiplexer," Opt. Express **22**, 84–89 (2014).
27. M. Shoeiby, A. Mitchell, and L. Bui, "Real time all optical correlator for serialized time encoded signals," Opt. Commun. **338**, 34–39 (2015).
28. A. E. Willner, A. Fallahpour, K. Zou, F. Alishahi, and H. Zhou, "Optical signal processing aided by optical frequency combs," IEEE J. Sel. Top. Quantum Electron. **27**, 1–16 (2021).
29. G. Bourdarot, H. G. de Chatellus, and J.-P. Berger, "Toward a large bandwidth photonic correlator for infrared heterodyne interferometry," Astron. Astrophys. **639**, A53 (2020).
30. P. Ambs, "Optical computing: a 60-year adventure," Adv. Opt. Technol. **2010**, 372652 (2010).
31. T. Manzur, J. Zeller, and S. Serati, "Optical correlator based target detection, recognition, classification, and tracking," Appl. Opt. **51**, 4976–4983 (2012).
32. P. M. Blanchard, A. H. Greenaway, A. R. Harvey, and K. Webster, "Coherent optical beam forming with passive millimeter-wave arrays," J. Lightwave Technol. **17**, 418–425 (1999).
33. C. A. Schuetz, R. D. Martin, I. Biswas, M. S. Mirotznik, S. Shi, G. J. Schneider, J. Murakowski, and D. W. Prather, "Sparse aperture millimeter-wave imaging using optical detection and correlation techniques," Proc. SPIE **6548**, 65480B (2007).
34. C. Wang, X. Xin, M. Kashif, and J. Miao, "A compact analog complex cross-correlator for passive millimeter-wave imager," IEEE Trans. Instrum. Meas. **66**, 2997–3006 (2017).
35. K. D. Merkel, J. T. Jackson, R. M. Price, W. R. Babbitt, C. Benko, S. H. Bekker, K. N. Winn, C. R. Stiffler, A. J. Woidtke, J. Oset, A. S. Traxinger, J. Salveson, M. D. Chase, P. B. Sellin, R. K. Mohan, and Z. W. Barber, "A photonics-based broadband RF spectrum analysis and geolocation system," in *IEEE Research and Applications of Photonics in Defense Conference (RAPID)* (2018), pp. 1–4.
36. W. R. Babbitt, "Microwave photonic processing with spatial-spectral holographic materials," Proc. SPIE **11296**, 112963L (2020).
37. CNRS/Université Grenoble Alpes, "Dispositif large-bande de mesure de la corrélation croisée de signaux," France patent FR2012782 (7 December 2020).

38. H. G. de Chatellus, E. Lacot, W. Glastre, O. Jacquin, and O. Hugon, "Theory of Talbot lasers," Phys. Rev. A **88**, 033828 (2013).
39. H. G. de Chatellus, O. Jacquin, O. Hugon, W. Glastre, E. Lacot, and J. Marklof, "Generation of ultrahigh and tunable repetition rates in CW injection-seeded frequency-shifted feedback lasers," Opt. Express **21**, 15065–15074 (2013).
40. H. G. de Chatellus, L. Romero Cortés, and J. Azana, "Optical real-time Fourier transformation with kilohertz resolutions," Optica **3**, 1–8 (2016).
41. C. Schnébelin and H. G. de Chatellus, "Agile photonic fractional Fourier transformation of optical and RF signals," Optica **4**, 907–910 (2017).
42. H. G. de Chatellus, L. Romero Cortés, C. Schnébelin, M. Burla, and J. Azaña, "Reconfigurable photonic generation of broadband chirped waveforms using a single CW laser and low-frequency electronics," Nat. Commun. **9**, 2438 (2018).
43. C. Schnébelin, J. Azana, and H. G. de Chatellus, "Programmable broadband optical field spectral shaping with megahertz resolution using a simple frequency shifting loop," Nat. Commun. **10**, 4654 (2019).
44. V. Duran, C. Schnébelin, and H. G. de Chatellus, "Coherent multiheterodyne spectroscopy using acousto-optic frequency combs," Opt. Express **26**, 13800–13809 (2018).
45. J. Clement, C. Schnébelin, H. G. de Chatellus, and C. R. Fernández-Pousa, "Laser ranging using coherent pulse compression with frequency shifting loops," Opt. Express **27**, 12000–12010 (2019).
46. V. Duran, L. Djevarhidjian, and H. G. de Chatellus, "Bidirectional frequency-shifting loop for dual-comb spectroscopy," Opt. Lett. **44**, 3789–3792 (2019).
47. V. Billault, V. Duran, C. R. Fernández-Pousa, V. Crozatier, D. Dolfi, and H. G. de Chatellus, "All-optical coherent pulse compression for dynamic laser ranging using an acousto-optic dual comb," Opt. Express **29**, 21369–21385 (2021).
48. I. Coddington, N. Newbury, and W. Swann, "Dual-comb spectroscopy," Optica **3**, 414–426 (2016).
49. N. Picqué and T. W. Hänsch, "Frequency comb spectroscopy," Nat. Photonics **13**, 146–157 (2019).
50. N. Kanagaraj, L. Djevarhidjian, V. Duran, C. Schnebelin, and H. G. de Chatellus, "Optimization of acousto-optic optical frequency combs," Opt. Express **27**, 14842–14852 (2019).
51. L. Shao, N. Sinclair, J. Leatham, Y. Hu, M. Yu, T. Turpin, D. Crowe, and M. Lončar, "Integrated microwave acousto-optic frequency shifter on thin-film lithium niobate," Opt. Express **28**, 23728–23738 (2020).